

ANALYSIS OF LIQUEFACTION INDUCED RESIDUAL DEFORMATION FOR TWO TYPES OF QUAY WALLS: ANALYSIS BY “FLIP”

Shun-ichi SAWADA¹, Osamu OZUTSUMI² And Susumu IAI³

SUMMARY

This paper presents the results of simultaneous analysis using the effective stress model called “FLIP (Finite element analysis of Liquefaction Program) [Iai, 1988]”. The effective stress model used for the analysis was a strain space multiple mechanism model, which takes into account the effect of rotation of principal stress axis during cyclic loading. Analyses were performed on two type quay walls to verify the liquefaction induced residual deformation. One is a sheet pile type quay wall at Showa-ohashi site during 1964 Niigata earthquake and the other is a caisson type quay wall at Uozaki-hama site during 1995 Hyogoken-nambu earthquake. Results of the finite element analysis are basically consistent with the observed performance of the quay walls.

INTRODUCTION

It is still fresh in our memories that quay walls in Kobe Port were greatly damaged during 1995 Hyogoken-nambu earthquake. The major cause of this damage was liquefaction-induced large ground displacement. Many numerical investigations have been conducted after the earthquake in order to investigate the mechanism of the movement of quay walls and to verify the applicability of the numerical technique. These efforts gradually have made the mechanism clear. Interested point in each research may, however, be different to each other, therefore it is sometimes difficult to obtain general feature of damage through these researches. The Technical Committee on Flow Deformation and Permanent Displacement of Ground and Earth Structures during Earthquakes, Japanese Geotechnical Society, planned simultaneous model tests and numerical analyses on the quay wall and backfill ground in order to grasp the general feature of damage [Kanatani and Yoshida, 1998]. This research was conducted as a part of this simultaneous analysis. Since detailed condition of the simultaneous analysis and general feature of the damage is discussed by Kanatani et al. [2000], result obtained by the numerical analysis are focused in this report.

2. OUTLINE OF EFFECTIVE STRESS MODEL

The analysis technique used in this study is classified into stress process method. This effective stress model is composed of two important models. One is the multi-springs model with hyperbolic nonlinear spring defined in strain space which takes into account the effect of rotation of principal stress axis directions, the effect of which is known to play an important role in the cyclic behavior of the anisotropy consolidated sand [Iai et al, 1992a&b]. A schematic figure is shown in Figure 2-1. The multi-spring model expects that hypothetical simple shear mechanism is generated with respect to the shearing section to which a hyperbola model applies. Use of this model allows the characteristic of hysteresis loops of multiple inelastic springs under the drained condition to be more similar to the results of laboratory tests. And this effective stress model extends the Masing rule to allow a desirable adjustment of historical loop size. The other is the excess pore water pressure model with a

¹ OYO corporation, Tokyo branch, Geotechnical Department., Tokyo, Japan Email: sawada-shun@oyonet.oyo.co.jp

² Institute of Japanese Union of Scientists & Engineers., Tokyo, Japan Email: ozutsumi@i-juse.co.jp

³ 3 Port and Harbour Research Institute, Ministry of Transport., Yokosuka, Japan Email: iai@cc.phri.go.jp

function of the normalized plastic shear work and shear stress. A schematic figure is shown in Figure 2-2. Excess pore water pressure is generated as a function of cumulative shear work. Effect of positive dilatancy is also included for taking into account the cyclic mobility behavior through the concept of liquefaction front defined in the effective stress space. The model can simulate the rapid or gradual increase in cyclic strain amplitude of the order of several percent under undrained cyclic loading.

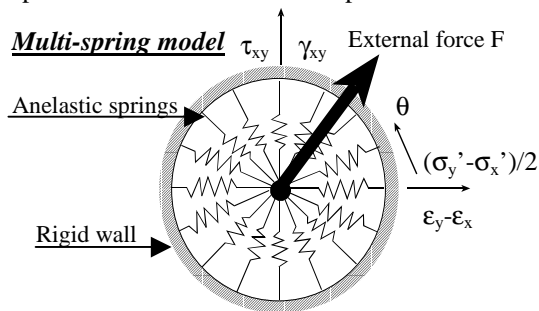


Figure 2-1: Schematic figure of multi-spring model

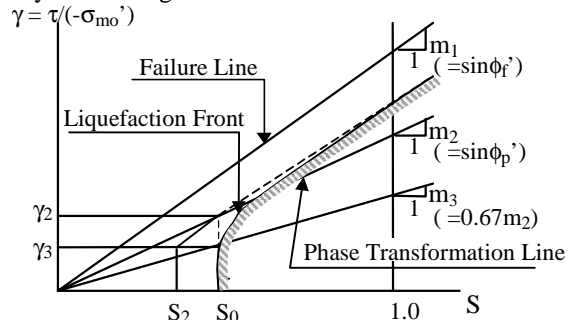


Figure 2-2: Schematic figure of liquefaction front, state variable S and shear stress ratio γ

3. SHOWA-OHASHI SITE

The Showa-ohashi site was damaged during 1964 Niigata earthquake. The horizontal residual displacement of the left riverside where was the sheet pile type quay wall was about 5m toward the river [Hamada, 1986]. The analysis model and analysis conditions were set up according to the simultaneous model shown by The Technical Committee on Flow Deformation and Permanent Displacement of Ground and Earth Structures during Earthquakes, Japanese Geotechnical Society [Kanatani and Yoshida, 1998].

3.1 Finite element modeling

Figure 3-1 shows soil profile and FE mesh. The subsoil is modeled into only rectangular elements. The sheet pile quay walls are modeled into linear beam elements. The bottom end of the sheet pile does not share the soil layer of $N=15$. The relative sliding and separation between the ground and quay wall is taken into account by the joint elements. The hydrodynamic pressure acting along the riverside of the quay wall is not considered, because their influence is slightly. The viscous boundary is set at the bottom of the model in order to consider the effect of semi-infinite region beneath the ground.

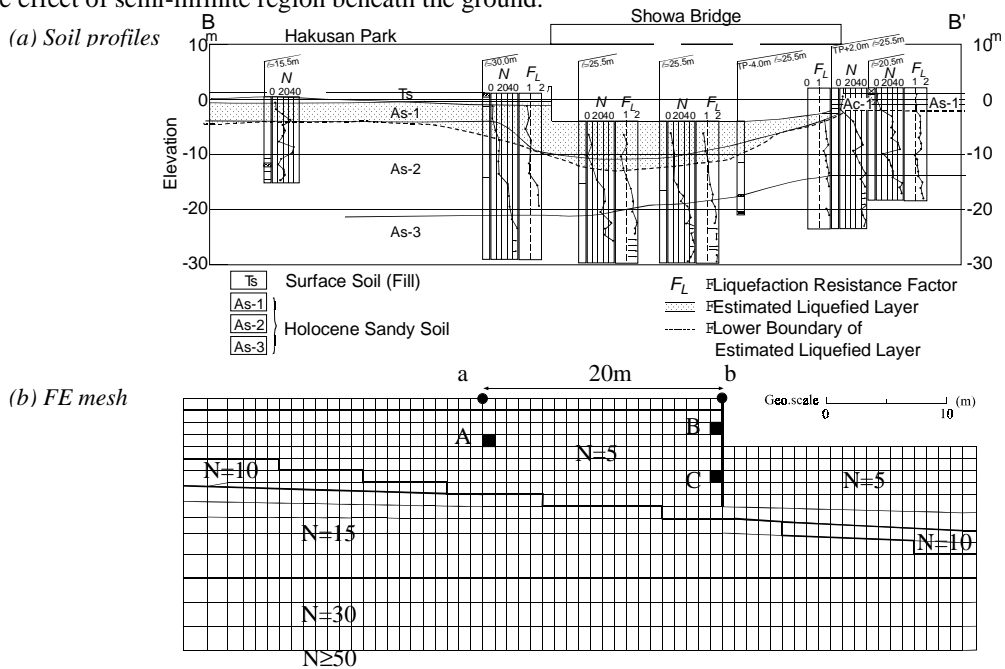


Figure 3-1: Soil profiles and FE mesh at Showa-ohashi site

3.2 Material properties

Material properties of soils and quay wall are given in Tables 3-1 and 3-2, respectively. This effective stress model requires the initial shear modulus (G_{ma}) depend on the initial mean effective stress (σ_{ma}'). To express σ_{ma}'

is obtained by assuming a coefficient of earth pressure at rest to be 0.5. The shear modulus for V_s is considered to G_{ma} as a reference. The shear modulus is proportional 0.5 times as much as the mean effective stress. Table 3-1 also lists liquefaction parameters defined by the trial and error process. Figure 3-2 compares the relationships between stress ratio (τ_d/σ_{mo}') and number of cycles to initial liquefaction obtained from the laboratory test and computed by using relevant parameters. Here, τ_d denotes shear stress amplitude and σ_{mo}' is initial effective confining stress. It is seen that computed result agrees with target almost perfectly.

Table 3-1: Material properties of soils

Soil layer	Surface	N=5	N=10	N=15	N=30
Initial shear velocity V_s (m/s)	110	140	180	200	240
Initial mean effective stress σ_{mo}' (kPa)	6.67	26.49	47.97	83.88	135.77
Initial shear modulus G_{mo} (kPa)	21797.82	37278.00	61626.42	80079.03	121084.83
Initial bulk modulus K_{mo} (kPa)	56858.76	97217.10	160707.42	208845.09	315764.28
Wet unit weight ρ_t (tf/m ³)	1.80	1.90	1.90	2.00	2.10
Porosity n	0.46	0.46	0.46	0.46	0.46
Maximum damping coefficient h_{max}	0.24	0.24	0.24	0.24	0.24
Internal friction angle ϕ_2' (deg.)	30.00	38.00	41.00	41.00	42.00
Liquefaction resistance ratio R_5	-	0.26	0.30	0.50	-
R_{20}	-	0.22	0.23	0.30	-
Phase transformation angle ϕ_{ps}' (deg.)	-	30.00	30.00	29.00	-
Ultimate limit of dilatancy S_1	-	0.0001	0.0001	0.0001	-
Overall cumulative dilatancy w_1	-	5.00	5.30	12.00	-
Initial phase of cumulative dilatancy p_1	-	0.50	0.50	0.50	-
Final phase of cumulative dilatancy p_2	-	1.10	0.98	0.90	-
Threshold limit for dilatancy c_1	-	2.37	2.20	2.20	-

Table 3-2: Material properties of quay wall

Sectional area	(cm ² /m)	153.00
Second moment of inertia	(cm ⁴ /m)	8740.00
Section modulus	(cm ³ /m)	874.00

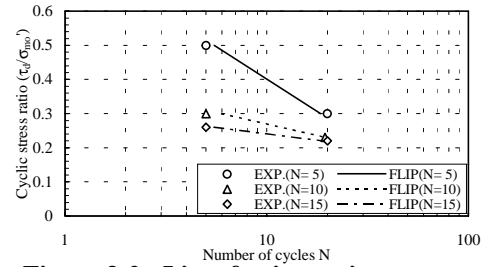


Figure 3-2: Liquefaction resistance curves

3.3 Input earthquake motion and numerical method

The input earthquake motion is the NS component of the Akita Prefecture Office at the underground floor accelerometer recorded during 1964 Niigata earthquake. The maximum acceleration of input earthquake motion is adopted to 120cm/s² (2E); it is given to the viscous boundary of the analysis model bottom.

The time integration is numerically done using the Wilson- θ method ($\theta = 1.4$). Rayleigh damping ($\alpha = 0.0$, $\beta = 0.003$), which is proportionally decreasing with the degree of cyclic mobility, is used to ensure stability of the numerical solution process.

3.4 Results of Analysis

3.4.1 Deformation

Figure 3-3 shows the calculated residual deformation near the quay wall at the end of the analysis, at 20 seconds. The residual horizontal displacement is 3.35m toward the river and the settlement is 4.59m. Figure 3-3 indicates that the residual deformation occurred only for the N=5 soil layer at the neighborhood of the quay wall. Figure 3-4 shows distributions of residual displacements on soil surface and riverbed in both horizontal and vertical directions. These figures show that the affected area from the quay wall is ± 20 m.

The residual horizontal displacement obtained well agreed to the actually observed.

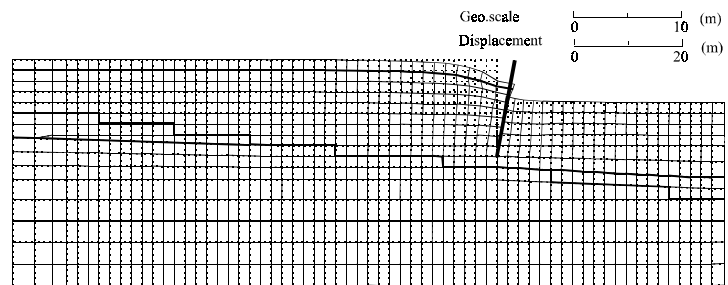


Figure 3-3: Residual deformation (near the quay wall)

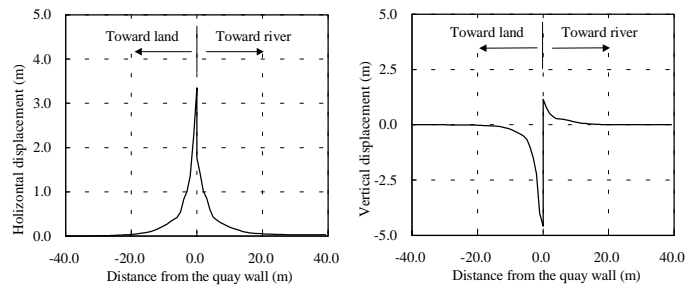


Figure 3-4: Distributions of residual displacement in both horizontal and vertical

3.4.2 Moment Distribution of Sheet Pile

Figure 3-5 shows the diagram of maximum bending moment of sheet pile per meter of wall width. The residual bending moment is almost the same as maximum. At a location of GL-6m in depth, the maximum bending moment is 461kNm/m, which exceeds the yield moment. But the calculated bending moment is not accurate after exceeding the yield moment, because the linear beam element is used for modeling of sheet pile.

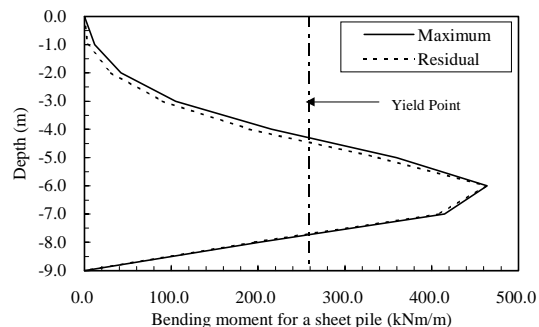


Figure 3-5: Bending moments of sheet pile

3.4.3 Excess pore water pressure

Figure 3-6 shows the distribution of maximum excess pore water pressure ratio ($1 - \sigma'_m / \sigma'_{mo}$) near the quay wall. The darkest part of the illustration represents the range where the excess pore water pressure ratio exceeds 0.9. This shows the elements where the excess pore water pressure ratio exceeds 0.9 are only the N=5 layer. On the other hand, a part of the N=5 layer which are lower than the riverbed behind the sheet pile indicate the excess pore water pressure ratio do not almost increase. Figure 3-7 shows the excess pore water pressure ratio time histories of elements A, B and C (See Figure 3-1). The time history of excess pore water pressure ratio for element A far away behind quay wall is gradually increased to the ratio of 0.9 for about 8 seconds and then keep the high values until the end of earthquake. However, for element B at the upper side behind the sheet pile, this ratio rapidly increases right after earthquake. On the other hand, for element C at the lower side behind the sheet pile, the excess pore water pressure ratio does not almost increase.

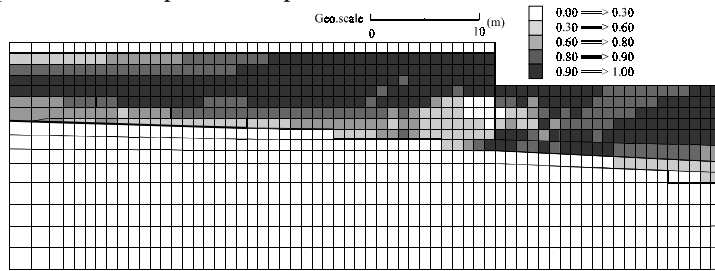


Figure 3-6: Maximum excess pore water pressure ratio (near the quay wall)

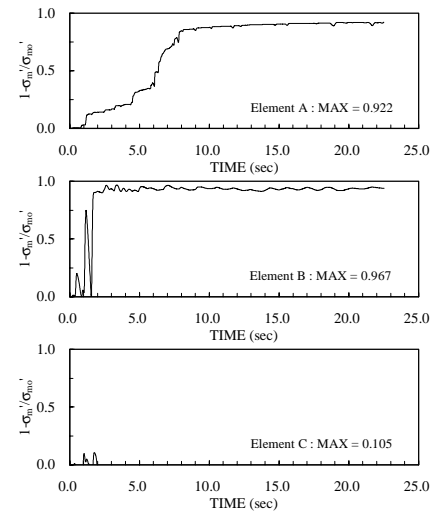


Figure 3-7: Time history of excess pore water pressure ratio

3.4.4 Time history of displacement and acceleration

Figure 3-8 shows time histories of relative displacement in horizontal and vertical directions on the surface of the land behind the sheet pile. Figure 3-9 shows the time histories of acceleration in horizontal and vertical directions on the surface 20m behind the quay wall (node a) and right behind the quay wall (node b).

At the node a, the maximum horizontal acceleration is 126 cm/s^2 , while that of vertical acceleration is 23 cm/s^2 . When the horizontal acceleration time history has passed 8 seconds, the amplitude became smaller. Around this time the major motion stopped, the element is N=5 layer for away from quay wall, and excess pore water pressure ratio is at its peak. So, the acceleration amplitude is considered smaller. On the surface right behind the sheet pile (node b), since there are spiky peaks attributable to close together and leave between sheet pile and soils, accelerations of over 800 to 1000 cm/s^2 are calculated in both horizontal and vertical directions. At the later parts of time history period became longer (about 1.4 second), and acceleration amplitude does not attenuate so much.

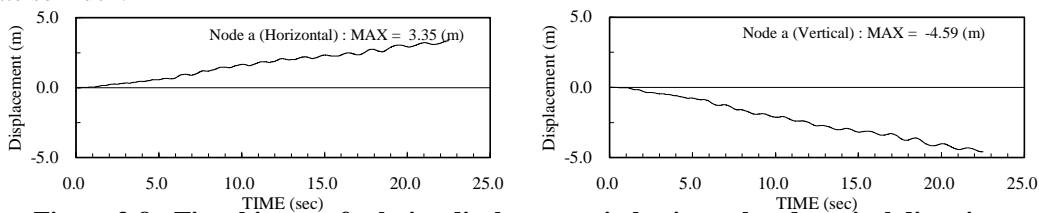


Figure 3-8: Time history of relative displacement in horizontal and vertical directions

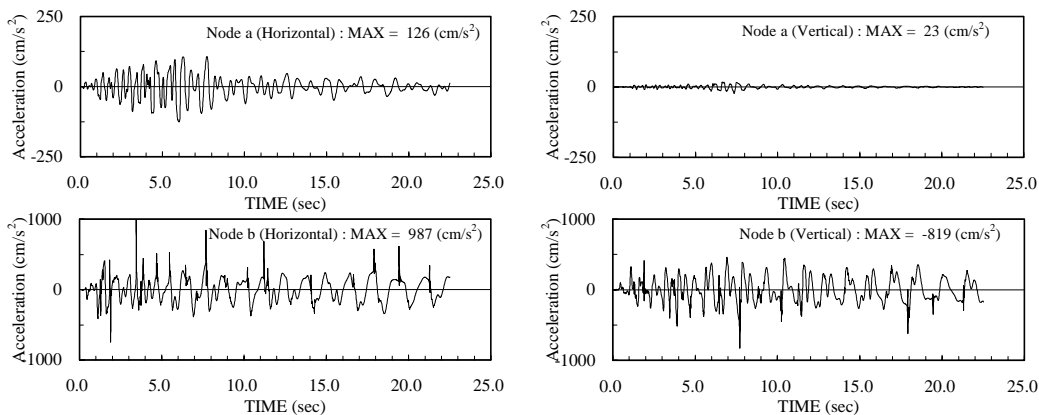


Figure 3-9: Time history of acceleration in horizontal and vertical directions

4. UOZAKI-HAMA SITE

The Uozaki-hama site was damaged during 1995 Hyogoken-nambu earthquake. The maximum horizontal residual displacement of 3.8m was observed at the south side quay wall of Uozaki-hama [Hamada, 1995]. The location that the simultaneous analysis considered is located near the Rokko-island Bridge. On this location, there is the pier with pile foundation for the bridge behind the caisson type quay wall. Deformation analysis using FLIP was conducted. The analysis model and conditions are set up according to the simultaneous model shown by The Technical Committee on Flow Deformation and Permanent Displacement of Ground and Earth Structures during Earthquakes, Japanese Geotechnical Society [Kanatani and Yoshida, 1998].

4.1 Finite element modeling

Figure 4-1 shows soil profile and FE mesh. The subsoil is modeled into only rectangular elements. The pier, footing and piles are modeled into linear beam elements. The bottom ends of the piles do not share the bottom of the model. The relative sliding and separation between the caisson and ground are considered by use of joint elements. The hydrodynamic pressure acting along the sea face of the caisson is taken into account using fluid elements.

4.2 Material properties

Material properties and model parameters are shown Table 4-1. The liquefaction parameters S_1 , w_1 , p_1 , p_2 and c_1 , in addition to phase transformation angle ϕ_p defined by the trial and error process to fit to the relation between stress ratios (τ_d/σ_{mo}) and the number of cycles to initial liquefaction. These liquefaction parameters are obtained by the element simulation based on the results of cyclic undrained triaxial tests using frozen samples at the Rokko Island. Figure 4-2 is seen that computed result agree with target almost perfectly. Table 4-1 also shows liquefaction parameters obtained.

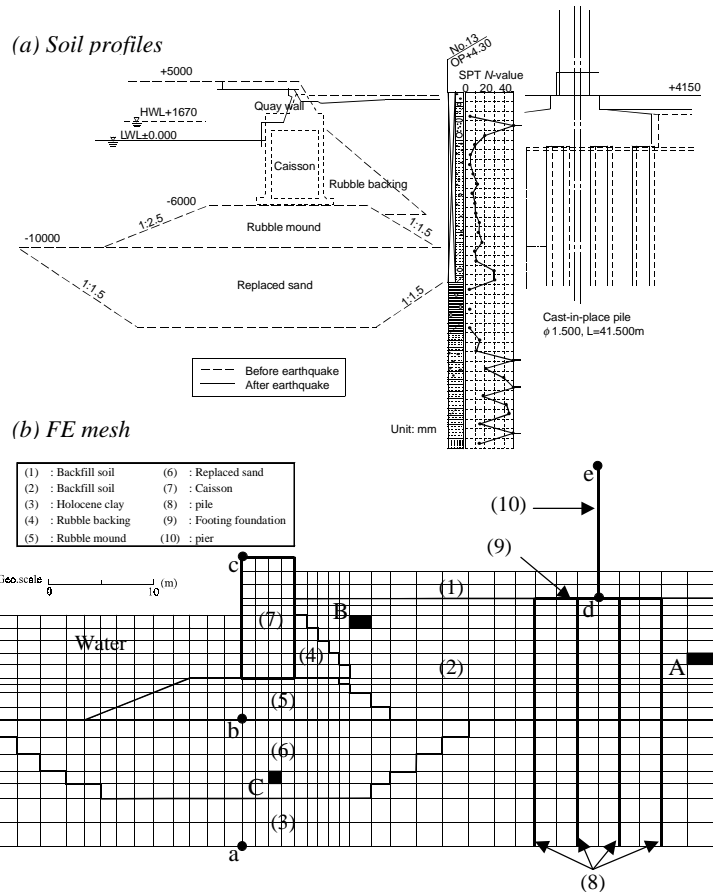


Figure 4-1: Soil profiles and FE mesh at Uozaki-hama site

Table 4-1: Material properties

Soil layer	(1)	(2)	(3)	(4)	(5)	(6)	(7)
Initial mean effective stress σ_{m0} (kPa)	17.22	77.11	172.15	9.81	9.81	57.03	-
Initial shear modulus G_m (kPa)	38749.50	82001.79	53523.36	180111.60	180111.60	70533.90	-
Initial bulk modulus K_m (kPa)	103318.92	218664.90	142735.50	480297.60	480297.60	188038.08	-
Wet unit weight ρ_t (tf/m ³)	1.80	2.00	1.60	2.00	2.00	2.00	2.10
Porosity n	0.46	0.46	0.55	0.46	0.46	0.46	-
Maximum damping coefficient h_{max}	0.24	0.24	0.30	0.24	0.24	0.24	-
Internal friction angle ϕ'_p (deg.)	37.00	37.00	30.00	40.00	40.00	37.00	-
Young's modulus E (kPa)	-	-	-	-	-	-	3.04E+07
Poisson's ratio ν	0.33	0.33	0.33	0.33	0.33	0.33	0.20
Liquefaction resistance ratio R_z	-	0.22	-	-	-	0.22	-
R_{30}	-	0.30	-	-	-	0.30	-
Phase transformation angle ϕ_p (deg.)	-	32.00	-	-	-	32.00	-
Ultimate limit of dilatancy S_1	-	0.005	-	-	-	0.005	-
Overall cumulative dilatancy w_1	-	5.00	-	-	-	4.50	-
Initial phase of cumulative dilatancy p_1	-	0.50	-	-	-	0.50	-
Final phase of cumulative dilatancy p_2	-	0.60	-	-	-	0.60	-
Threshold limit for dilatancy c_1	-	2.40	-	-	-	2.40	-
Pier, footing and piles							
Shear modulus G (kPa)	1.02E+07	1.02E+07	1.02E+07				
Poisson's ratio ν	0.20	0.20	0.20				
Unit weight ρ_t (tf/m ³)	2.40	2.40	2.40				
Sectional area (m ²)	0.452	3.600	3.600				
Second moment of inertia (m ⁴)	0.063	3.888	3.573				

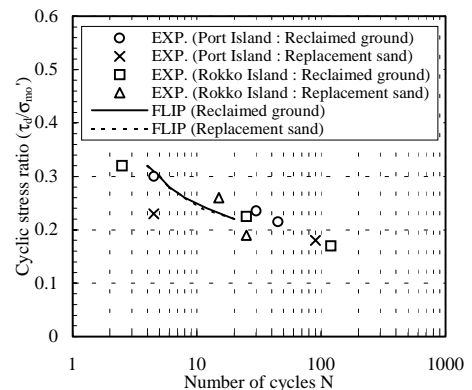


Figure 4-2: Liquefaction resistance curves

4.3 Input earthquake motion and numerical method

The NS component of the Port-Island accelerogram at GL-16.4m recorded during 1995 Hyogoken-nambu earthquake is used as input motion. This waveform is time interval of 0.01 second, number of 2048 data and peak acceleration of 565 cm/s^2 (E+F). The time integration is numerically done using the Wilson- θ method ($\theta = 1.4$). Rayleigh damping ($\alpha = 0.0$, $\beta = 0.005$), which is proportionally decreasing with the degree of cyclic mobility, is used to ensure stability of the numerical solution process.

4.4 Results of analysis

4.4.1 Deformation

The results of effective stress analysis of the quay wall at Uozaki-hama site in the deformation near the quay wall shown in Figure 4-3, deformations towards the sea are mainly seen at the replaced sand under the caisson and backfill behind the caisson. The residual horizontal displacement at the top of the caisson is 2.98m seaward whereas the observed displacement range from about 2.0 to 3.8m, indicating the calculated displacement is consistent with those observed. And the calculated settlement is 1.1m and calculated rocking angle is 5 degrees. The caisson is stuck into the rubble mound and deformed, resulting in continuous deformation of the replaced sand and the backfill behind the caisson. At the same time, the horizontal displacement at the bottom of pier behind the caisson is 34cm, which is attributable to the deformation of the caisson toward the sea. Figure 4-4 shows the relation between distance from waterfront and the distribution of residual horizontal displacement at the points of surface. This distribution is not significant due to the pier foundation, however, the affected area from waterfront of the residual horizontal displacement is about 80m.

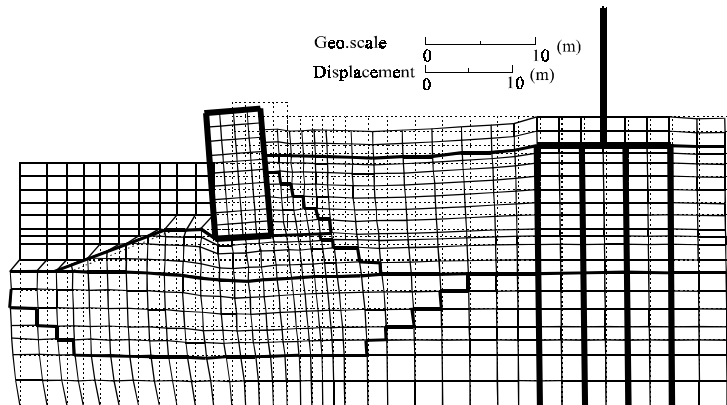


Figure 4-3: Residual deformation (near the quay wall)

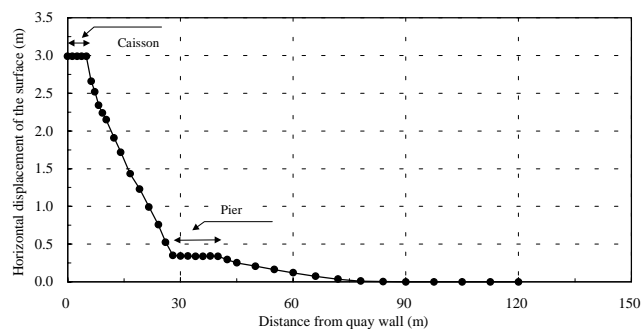


Figure 4-4: The surface distribution of residual horizontal displacement

4.4.2 Bending moment

Figure 4-5 shows the maximum bending moments of the bridge pile foundation. This analysis assumes that piles are constructed by cast-in-place type reinforced concrete and the fixed condition of piles at the footing joint and bottom end are pin support. As the result of analysis, the maximum bending moment on the pile generates in the Holocene clay right down the backfill where the excess pore water pressure raised. The maximum bending moment for each pile is 9339 kNm/pile, which much exceeded the yield moment. Since the pile is modeled as a liner beam element, the analysis underestimated the residual deformation of the ground.

Table 4-2: Various moments

Moment		(kNm/pile)
Crack Moment	M_c''	1226.25
Yield moment	M_y''	2648.70
Failure moment	M_u''	3737.61

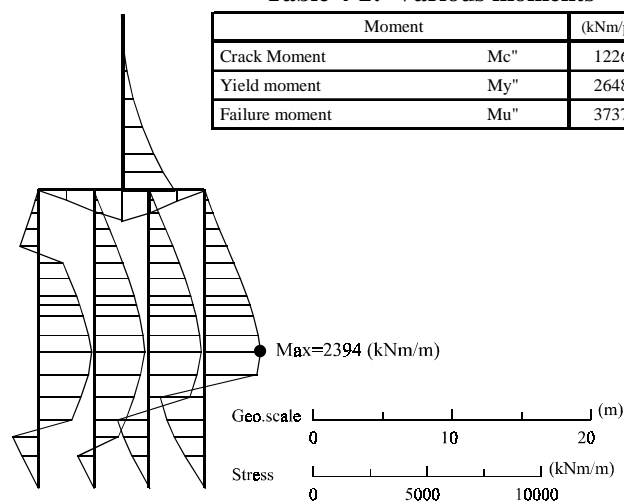


Figure 4-5: Maximum bending moments of the bridge pile foundation

4.4.3 Excess pore water pressure

Figure 4-6 shows the distribution of computed excess pore water pressure ratio near the quay wall at the end of shaking. Excess pore water pressure ratio exceeds 0.9 are elements where the backfill far away from the caisson.

On the other hand, the parts of the replaced sand layer and the backfill right behind of the caisson indicate the excess pore water pressure ratio do not almost increase at the end of shaking. Figure 4-7 shows the time histories of the excess pore water pressure ratio. At element A of the backfill far away from the caisson, the excess pore water pressures ratio gradually increased to a level of 0.9 or more. And after 10 seconds, the value remained. However, the excess pore water pressure ratio varies drastically according to caisson deformation at elements B and C. The residual excess pore water pressure ratios do not exceed 0.5.

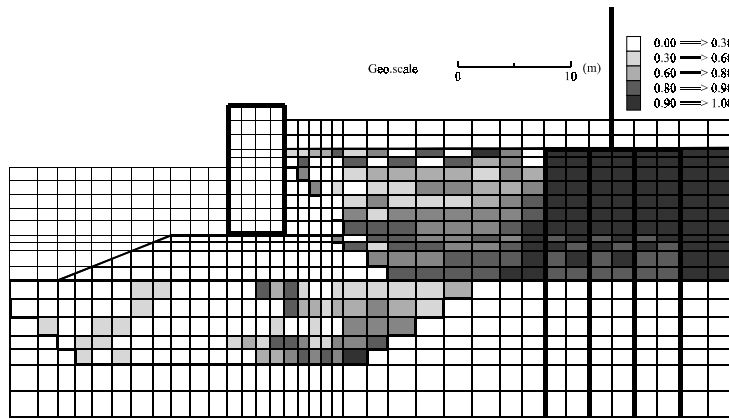


Figure 4-6: Residual excess pore water pressure ratio (near the quay wall)

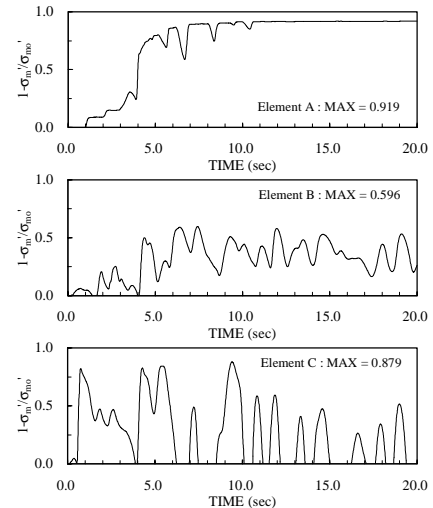


Figure 4-7: Time history of excess pore water pressure ratio

4.4.4 Time history of displacement and acceleration

Figure 4-8 shows the time histories of horizontal and vertical displacement at the nodes of *c* to *e* indicated in Figure 4-1. Figure 4-9 shows a time histories of horizontal acceleration at the nodes of *a* to *d*. The maximum horizontal displacement at the top of the caisson is 2.98m toward the sea at the end of shaking. And the calculated settlement is 1.18m. The displacement at the node of *c* begins right after the major motion. It moved drastically toward the sea after about 6 seconds when the input acceleration became its maximum. It moved only into a single direction (toward the sea), but moved back toward in the opposite direction (toward the land). Thus the displacement finally moved toward the sea. At the bridge pier foundation, there is a residual horizontal displacement of 53cm toward the sea. The reason why the residual deformation at the pier foundation is less than the caisson is that the shearing stiffness of the soil layer around the pile foundation decreased, as the excess pore water pressure of the backfill increased. This allowed the deformation to be improved by the elastic restoration of the modeled pile with linear beam elements. The maximum horizontal displacement at the top of bridge pier is 54cm toward the sea at 8.27 seconds. This phenomenon well agrees with the observed damage of the top of Rokko-island Bridge pier.

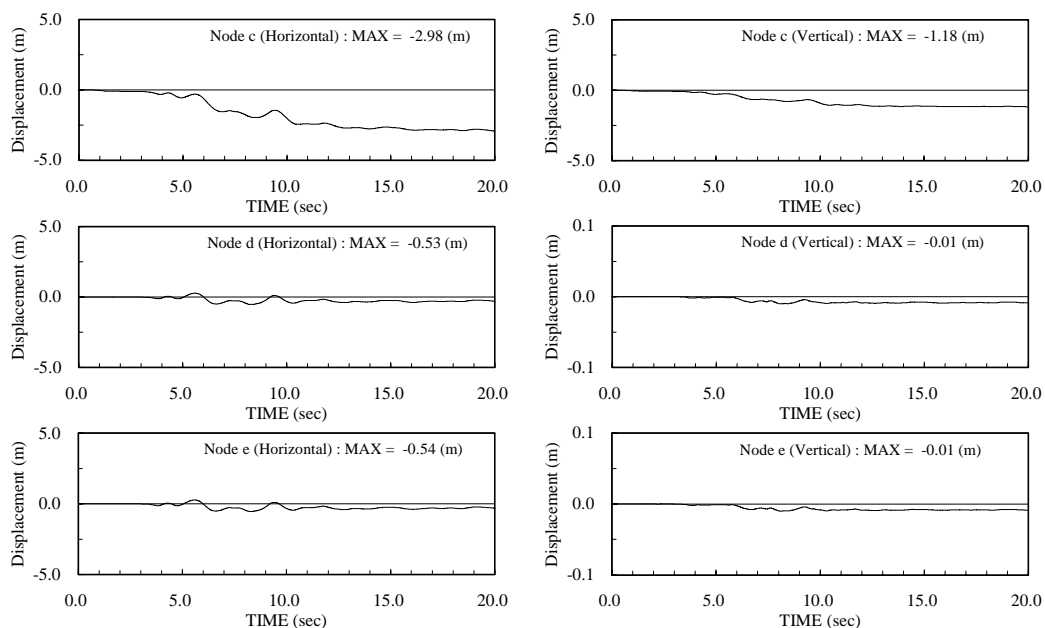


Figure 4-8: Time history of relative displacement in horizontal and vertical directions

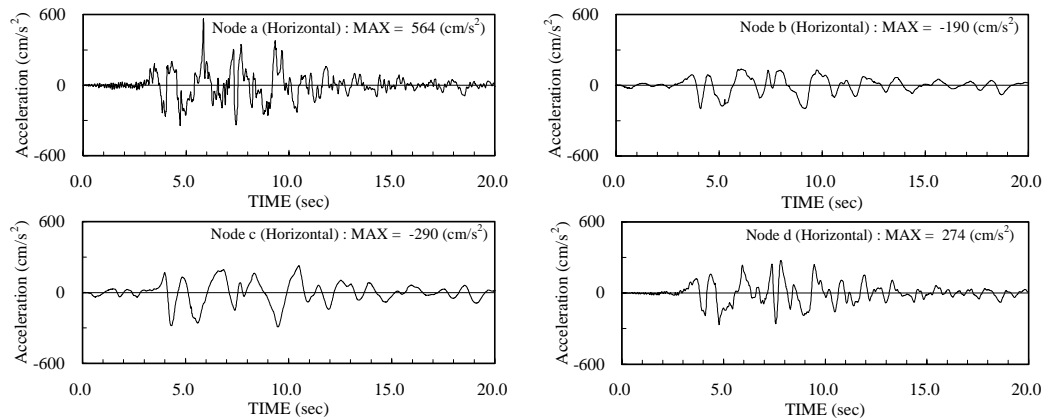


Figure 4-9: Time history of acceleration in horizontal and vertical directions

5. CONCLUSIONS

In this paper, the effective stress analysis using FLIP is performed for the dynamic response for two types of quay walls. One is the sheet pile type quay wall at Showa-ohashi site during 1964 Niigata earthquake and the other is the caisson type quay wall at Uozaki-hama site during 1995 Hyogoken-nambu earthquake. The results of the analysis were basically consistent with the observation of the liquefaction induced residual deformation. Based on these analyses, it is concluded that, the FLIP has the potential ability to simulate the liquefaction induced residual large deformation during earthquake.

6. REFERENCES

- Hamada, M., Yasuda, S., Isoyama, R. and Emoto, K. (1986), "Study of liquefaction induced permanent ground displacement", ADEP.
- Hamada, M., Wakamatsu, K. and Isoyama, R. (1995), "The 1995 Hyogoken-nambu (Kobe) Earthquake, Liquefaction, Ground displacement and soil condition in Hanshin area," ADEP.
- Iai, S. (1988), "A model that does not break out in the two-dimensional effective stress analysis for liquefaction," *Proc., 43rd Annual Conf. of JSCE*, 3, pp418-419 (in Japanese)
- Iai, S., Matsunaga, Y. and Kameoka, T. (1990), "Parameter identification for a cyclic mobility model," *Report of the Port and Harbour Research Institute*, Vol.29, No.4, pp.57-83
- Iai, S., Matsunaga, Y. and Kameoka, T. (1992a), "Strain apace plasticity model for cyclic mobility," *Soils and Foundations*, Vol.32, No.2, pp.1-15
- Iai, S., Matsunaga, Y. and Kameoka, T. (1992b), "Anaiysis of undrained cyclic behavior of sand under anisotropic consolidation," *Soils and Foundations*, Vol.32, No.2, pp.16-20
- Japanese Harbour Society Corporation (1989), "Design standard for port facilities" (in Japanese).
- Kobe City Development Bureau (1995), "Report of investigation for liquefaction-induced large ground displacement at reclaimed land (Port Island and Rokko Island)" (in Japanese).
- Kanatani, M. and Yoshida, N. (1998), "Simultaneous model tests and analyses on waterfront structure during earthquake," *Proc., Symp. on Flow and Permanent Displacement of Ground and Soil Structures during Earthquakes*, JGS, pp159-192 (in Japanese).
- Kanatani, M. and Yoshida, N. (1998), "Simultaneous model tests and analyses on waterfront structure during earthquake," *Proc., Symp. on Flow and Permanent Displacement of Ground and Soil Structures during Earthquakes*, JGS, pp159-192 (in Japanese).
- Kanatani, M., Yoshida, N. and Yasuda, S. (2000), "Simultaneous model tests on quay wall and liquefied backfill ground during earthquake" *Proc. 12WCEE* (to be published).